Flow-driven pattern formation in the calcium-oxalate system

Bíborka Bohner[1], Balázs Endrődi[1], Dezső Horváth[2], and Ágota Tóth[1*]

[1]*Department of Physical Chemistry and Materials Science, University of Szeged, Aradi vértanúk tere 1., Szeged, H-6720, Hungary*

[2]*Department of Applied and Environmental Chemistry, Rerrich Béla tér 1., Szeged, H-6720, Hungary*

(Dated: April 4, 2016)

Abstract

The precipitation reaction of calcium oxalate is studied experimentally in the presence of spatial gradients by controlled flow of calcium into oxalate solution. The density difference between the reactants leads to strong convection in the form of a gravity current that drives the spatiotemporal pattern formation. The phase diagram of the system is constructed, the evolving precipitate patterns are analyzed and quantitatively characterized by their diameters and the average height of the gravity flow. The compact structures of calcium oxalate monohydrate produced at low flow rates are replaced by the thermodynamically unstable calcium oxalate dihydrate favored in the presence of a strong gravity current.

*E-mail:atoth@chem.u-szeged.hu

I. INTRODUCTION

Self-organization in precipitation reactions like silica gardens[1] or Liesegang rings[2] has been known for centuries, yet recent developments in the newly emerging field of chemobrionics[3–5] bring attention again to the interaction of transport processes and chemical reactions leading to the formation of a solid material. A growing number of self-organized or self-assembled systems have been designed[6, 7], investigated[8, 9], controlled[10], and modeled[11] up to now because not only they are related to natural nonlinear phenomena but also they may provide novel pathways[4] in creating new materials[12] and introducing new technologies[13] unavailable in well-stirred systems. The presence of spatial gradients is the important characteristics of these systems that leads to the corresponding transport processes. If they are coupled to nonlinear kinetics, emergent behavior is observed because of the various instabilities far from thermodynamic equilibrium.[14, 15]. Even in simple inorganic reactions, delicate precipitate patterns may evolve through osmotic effects coupled with buoyancy[16–18], hydrodynamic instability due to viscous fingering[19], density gradients[3, 20], or surface tension gradients[21–23].

The interaction of a gravity current with a simple precipitation reaction may give rise to an unusual spatial distribution of solid copper oxalate.[24] As a result of the hydrodynamic instability at the tip of the flow and the slow kinetics of the precipitation, equidistantly spaced thin filaments rich in precipitate emerge radially from a local source (a pellet or an inlet). The local mixing at the leading edge of the gravity current, maintained by the density difference between the two fluids, and the spatially ordered sedimentation yield solid particles with morphology different from those obtained from the corresponding well-stirred system.[24, 25] With this flow-driven method we have been able to successfully synthesize calcite crystals selectively in the calcium–carbonate system, whereas a mixture of calcite and vaterite forms in the homogeneous reference case in the absence of gradients.[26] When dense calcium chloride solution is pumped into sodium oxalate solution, the flow maintained by the gravity current and the spatially localized nucleation of crystallization favor the formation of the thermodynamically unstable calcium oxalate dihydrate (COD).[27] Although it is frequently found in human kidney stones,[28] its synthetic production in the absence of spatial gradients is generally complicated because it requires various chemical stabilizers[29, 30] to suppress the formation of the stable monohydrate whewellite (COM).[31]

This manuscript was accepted by J. Chem. Phys. Click here to see the version of record.

In this detailed experimental work we study the flow-driven precipitate pattern formation in the calcium–oxalate system by systematic variation of the parameters affecting the underlying gravity current. By selecting the appropriate descriptors and identifying their dependence on the physical quantities that determine the flow pattern, we are able to characterize the spatiotemporal pattern formation, which, in this particular example, may help to optimize the production of the various calcium oxalate hydrates without any stabilizers. We complete the study of the spatially extended system with equilibrium calculations to obtain the concentration distribution of species, reference experiments of the well-stirred system, and analytical measurements.

II. EXPERIMENTAL

Reagent-grade chemicals and deionized water were used to prepare the reactant solutions of 1–4 mol/dm^3 calcium chloride (Scharlau) and 0.01–0.1 mol/dm^3 sodium oxalate (VWR). The sodium oxalate solution was always prepared in situ with its pH set to 9.0. In order to vary the characteristics of fluid motion, inert materials such as solid sodium chloride (Molar), solid polyvinyl alcohol (Sigma Aldrich), 50 m/m% solution of polyacrylamide (Aldrich), and glycerol (VWR) were also dissolved in the calcium chloride solution. The density of the mixtures were then determined with an Anton Paar DMA 500 digital density meter with 10^{-4} g/cm^3 precision, while the relative viscosity with respect to water was measured with an Ostwald viscometer. The density of the calcium chloride solution was always kept greater than that of the sodium oxalate as shown in Table I, which summarizes the density difference between the two reactant solutions without any additional material.

The flow-driven experiments were carried out in a horizontally leveled square glass reaction vessel (with sides of 24 cm) containing 250 cm^3 sodium oxalate solution, i.e., the depth of oxalate solution was 4.3 mm. Calcium chloride solution was injected at 2–100 mL/h flow rate from below, into the center of the dish through a circular opening created by a needle with 0.8 mm inner diameter sealed around with silicone adhesive. The needle was connected to a peristaltic pump (Ismatec Reglo) with thin Tygon tubes (inner diameter of 0.25 mm or 0.57 mm) to allow faster pump rotation and hence to minimize the fluctuations in the flow rate. In addition, for reference investigations, 50 cm^3 of one reactant was added dropwise into a continuously stirred beaker containing 50 cm^3 of the other one with a rigorous stirring

TABLE I: Density difference in g/cm^3 between the applied solutions of calcium chloride and sodium oxalate without any inert materials added to the calcium chloride solution.

	c(Calcium chloride) / (mol/dm^3)			
c(Sodium oxalate)	1.0	2.0	3.0	4.0
0.1 mol/dm^3	0.0780	0.1483	0.2064	0.3230
0.05 mol/dm^3	0.0833	0.1536	0.2117	0.3283
0.025 mol/dm^3	0.0860	0.1563	0.2144	0.3310
0.01 mol/dm^3	0.0861	0.1564	0.2145	0.3311

at 1000 rpm.

The evolution of precipitate patterns was monitored from above using a digital camera (Unibrain 1394) and analyzed by a computer-controlled imaging system with in-house software. The diameters of the inner (d_i) and the outer circle (d_o) associated with the precipitate disc, shown in Figure 1 at $t = 4$ min, were compared for various conditions. For each set of parameters five independent measurements were conducted in order to allow calculating the average and the standard deviation of these descriptors. The number of radially growing thin lines enriched in precipitate, termed filaments in this work, was counted manually from the grayscale intensity data, along a 90° circular arc where they were identified as local maxima in the grayscale values.

As a result of the substantial difference in fluid density in the presence of gravity, pressure equalization is achieved by the formation of a strong flow at the bottom of the fluid, known as gravity current or gravity flow. Since the precipitation reaction spatially localized to the horizontally spreading dense liquid layer, the precipitate pattern itself can be considered, in a sense, as a footprint of the gravity current. Its spatial extent in the horizontal plane corresponds to that of the gravity current, from which the average height of the latter ($\bar{h}$) can be obtained. It is defined as the ratio of the liquid volume (V) pumped in to the surface area (A) of the precipitate pattern with the following formula:

$$\bar{h} = \frac{V}{A} = \frac{4\,w\,t}{d_o^2\,\pi}, \tag{1}$$

where w is the flow rate at which the calcium chloride solution is pumped into the sodium oxalate solution, while d_o corresponds to the outer diameter of the precipitate at time t.

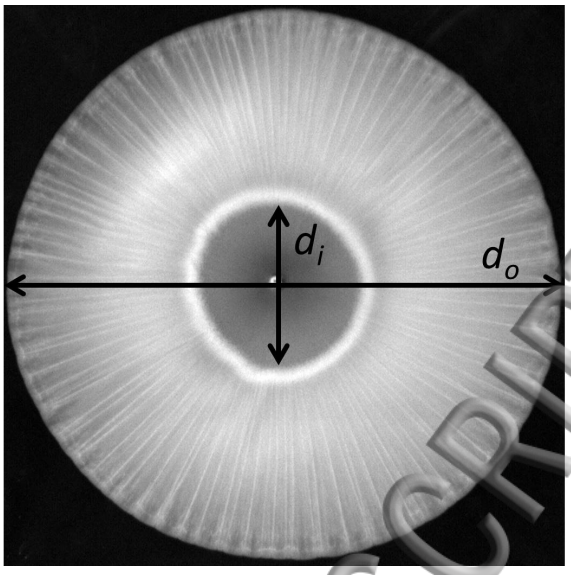

FIG. 1: The image of a calcium oxalate precipitate pattern at $t = 4$ min with indicating the quantitative descriptors: diameter of the inner (d_i) and the outer (d_o) circle. Experimental conditions are $[CaCl_2] = 4$ mol/dm^3, $[Na_2C_2O_4] = 0.025$ mol/dm^3, $w = 20$ mL/h.

After each experiment, the solution was removed without stirring by carefully pipetting out most of the liquid. The vessel with the remaining wet particles in it was left at room temperature for overnight allowing the complete evaporation of the solvent water. Then samples were collected from the inner and the outer parts of the precipitate pattern separately. The microstructure of the crystalline solid material was investigated using a field emission scanning electron microscope (Hitachi S-4700). The composition of the precipitate was determined by Raman spectroscopy (Bio-Rad Digilab Division Dedicated FT Raman) and the individual particles were analyzed with Raman microscopy (Thermo DXR Raman).

III. EQUILIBRIUM CALCULATIONS

The concentration distribution of the various species is calculated for pH range 0–14 by using the available solubility products, equilibrium constants for complex formation and protonation.[32] Besides the precipitation reactions leading to insoluble calcium oxalate and

This manuscript was accepted by J. Chem. Phys. Click here to see the version of record.

calcium hydroxide

$$Ca^{2+} + (COO)_2^{2-} \longrightarrow \underline{Ca(COO)_2} \qquad pK_{s_1} = 7.90 \qquad (2)$$

$$Ca^{2+} + 2OH^- \longrightarrow \underline{Ca(OH)_2} \qquad pK_{s_2} = 5.10 \qquad (3)$$

the complexation reactions with calcium ion,

$$Ca^{2+} + OH^- \rightleftharpoons CaOH^+ \qquad lg\beta_{OH} = 1.15 \qquad (4)$$

$$Ca^{2+} + (COO)_2^{2-} \rightleftharpoons Ca(COO)_2 \qquad lg\beta_1 = 1.66 \qquad (5)$$

$$Ca(COO)_2 + (COO)_2^{2-} \rightleftharpoons Ca[(COO)_2]_2^{2-} \qquad lg\beta_2 = 2.69 \qquad (6)$$

$$Ca^{2+} + HOOC - COO^- \rightleftharpoons Ca(HOOC - COO)^+ \qquad lg\beta_{H_1} = 1.38 \qquad (7)$$

$$Ca^{2+} + 2HOOC - COO^- \rightleftharpoons Ca(HOOC - COO)_2 \qquad lg\beta_{H_2} = 1.80 \qquad (8)$$

and the protonation equilibria of oxalate ion are considered

$$H^+ + (COO)_2^{2-} \rightleftharpoons HOOC - COO^- \qquad lgK_{H_1} = 4.266 \qquad (9)$$

$$H^+ + HOOC - COO^- \rightleftharpoons (COOH)_2 \qquad lgK_{H_2} = 1.252 \qquad (10)$$

The initial concentrations of the two solutions are set to $[CaCl_2] = 4$ mol/dm^3 or 1 mol/dm^3 and $[Na_2C_2O_4] = 0.025$ mol/dm^3 or 0.1 mol/dm^3, respectively. The component balance equations for calcium and oxalate are expressed and solved at constant pH with a preset accuracy of 10^{-14} using Wolfram Mathematica.

As illustrated in Figure 2, calcium oxalate precipitate is present in the system over the entire calculated pH range for the above conditions. Only calcium ion exists in significant amount, all complexes are negligible. Upon increasing the pH to 11, the concentration of $CaOH^+$ increases, while that of the $Ca(HOOC - COO)^+$ decreases. In strongly alkaline medium (pH $>$ 11) the insoluble calcium hydroxide dominates, therefore for obtaining pure calcium oxalate precipitate experimentally, the pH of the solution has to be set below pH = 11. In this region, the amount of calcium ion and $CaOH^+$ decreases, while the dioxalato complex of calcium increases four magnitude and its quantity becomes comparable to the former ones.

Upon increasing the excess of calcium used, the amount of calcium oxalate precipitate decreases with respect to that of calcium ion. Even more than tenfold increase in excess will only shift the appearance of hydroxide precipitate to slightly lower pH, thus the initial

This manuscript was accepted by J. Chem. Phys. Click here to see the version of record.

setting of pH to 9.0 is sufficiently robust for the entire concentration range used in our experimental work.

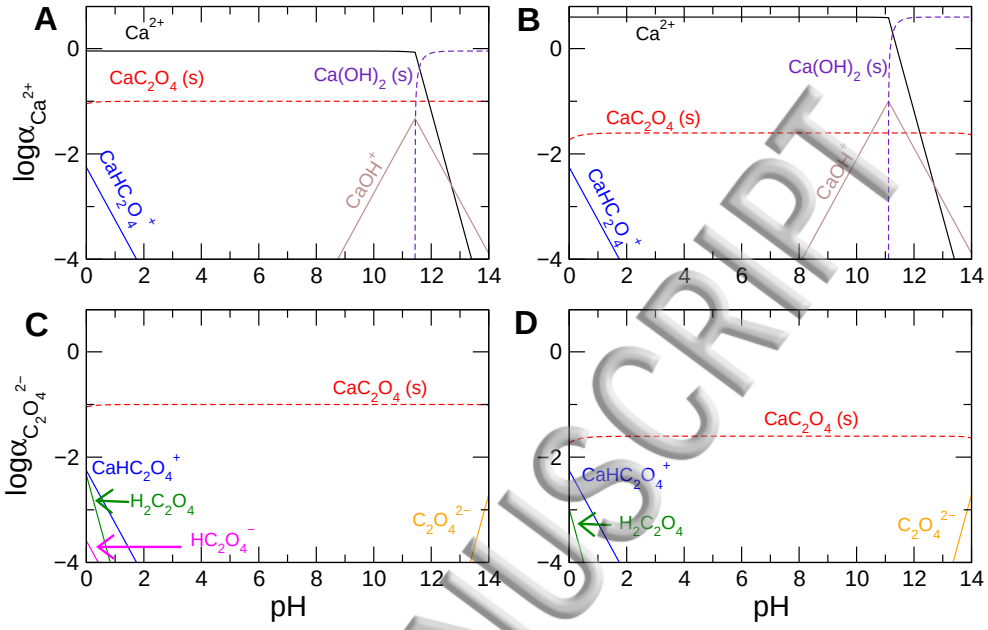

FIG. 2: The distribution of the Ca^{2+} and $C_2O_4^{2-}$ containing species calculated with $[CaCl_2] = 1$ mol/dm^3 (A, C) or 4 mol/dm^3 (B, D), $[Na_2C_2O_4] = 0.1$ mol/dm^3 (A, C) or 0.025 mol/dm^3 (B, D).

IV. RESULTS & DISCUSSION

In the well-stirred reference system, the mixing of reactants instantaneously results in the appearance of the white calcium oxalate precipitate. Immediate precipitation takes place in the flow-driven system as well, as the solution with greater density (i.e., typically the more concentrated solution) sinks to the bottom of the dish leading to the formation of a white precipitate pattern spreading around the small inlet where the calcium chloride solution is pumped in. The evolving pattern has two distinct regions: the inner circle around the orifice has less precipitate sedimentation, while the outer circular zone contains significantly more precipitate. In most cases there is a sharp transition between the darker inner and the brighter outer region (see Fig. 1). An angular variation in the precipitate quantity also develops in the outer region as radially oriented lines rich in calcium oxalate become visible

in the form of faint filaments. This is a result of hydrodynamic instability that develops behind the tip of the gravity current leading to alternating zones of downward and upward flow transverse to the direction of spreading. In the time scale of our experiments the number of filaments remains constant for a precipitate pattern, since no merging or splitting is observed. There is a small fluctuation in the spacing between the filaments as indicated by the experimental errors in the tables.

The spatial spreading of the precipitate pattern, quantified by the diameter of the inner and outer circles, depends on the density difference maintained, i.e., the concentrations of the reactant solutions. The observed patterns at $t = 4$ min at different chemical compositions are summarized in Fig. 3 where, in all cases, 20 mL/h flow rate is used and the pH of the sodium oxalate solution has been initially set to 9.

At a constant oxalate concentration, the increase of calcium ion concentration leads to circular patterns with increasing outer diameter (see Table II), which is attributed to the greater density difference between the two solutions that generates more intense fluid motion, i.e., a stronger gravity current. On contrary, keeping calcium ion concentration constant and increasing the oxalate concentration yield more compact patterns, since the density change between the solutions decreases and the gravity flow weakens. Furthermore, at the highest sodium oxalate concentrations applied in our experiments, the gravity current is diminished to the extent that the growth of precipitate pattern is accompanied by a significant loss of the circular symmetry. The absence of strong flow at these concentrations also leads to the disappearance of precipitate filaments.

Since at pH = 0–5 no significant precipitation takes place in the time scale of the experiment, we have checked the effect of pH on the rate of precipitate formation in a separate set of experiments. The temporal evolution of the characteristic diameters is monitored in the range $6 < \mathrm{pH} < 10$ with a chemical composition of $[CaCl_2] = 4$ mol/dm^3 and $[Na_2C_2O_4] = 0.025$ mol/dm^3. Figure 4 demonstrates that while both diameters vary independently of the pH, the diameter of the inner circle approaches a constant value in time, i.e., it can be used to characterize the evolving structure, whereas the diameter of the outer circle continually increases according to a square-root relationship of geometric spreading. The latter time-dependence reveals that the precipitate indeed grows with the gravity current underneath.

To demonstrate the significance of convection in the precipitate formation, we have varied

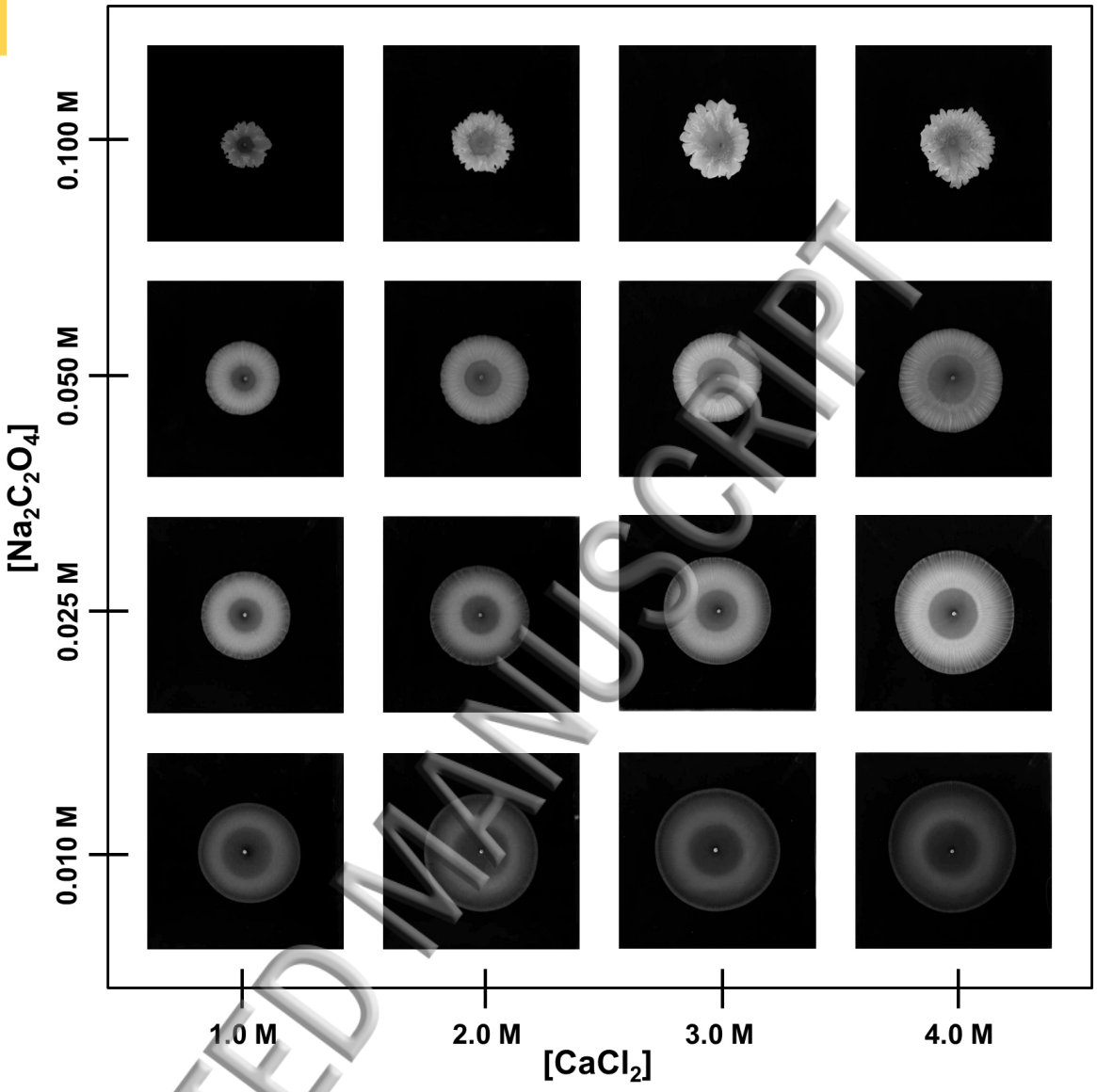

FIG. 3: Phase diagram associated with the calcium–oxalate system showing the precipitate pattern evolved at time $t = 4$ min with $w = 20$ mL/h. Field of view: 24 cm $\times$ 24 cm.

the flow characteristics. At first, the pattern descriptors are determined at various flow rates increasing from 2 to 100 mL/h. In the absence of sufficient gravity flow, irregularly shaped precipitate patterns emerge, only above $w = 10$ mL/h can we observe symmetric patterns. Upon increasing the flow rate, both the diameters of the precipitate disc and the number of radially growing filaments in the outer region increases as listed in Table III. In parallel, the average height of gravity flow also rises from 0.04 mm to 0.28 mm.

TABLE II: The influence of chemical composition on the characteristics of the precipitate pattern at time $t = 4$ min, with experimental errors given in brackets. Also listed in the last column is the calculated average height of the underlying gravity current.

Concentration		Pattern			
$CaCl_2$ (mol/dm^3)	$Na_2C_2O_4$ (mol/dm^3)	d_i (mm)	d_o (mm)	N	$\bar{h}$ (mm)
1	0.010	58 (1)	117 (2)	-	0.12
	0.025	40 (1)	103 (1)	-	0.16
	0.050	28 (1)	87 (1)	76 (4)	0.22
2	0.010	65 (3)	133 (1)	-	0.10
	0.025	47 (1)	118 (1)	112 (4)	0.12
	0.050	41 (1)	100 (1)	88 (4)	0.17
3	0.010	60 (1)	144 (1)	-	0.08
	0.025	49 (1)	128 (1)	100 (4)	0.10
	0.050	48 (2)	106 (2)	76 (4)	0.15
4	0.010	64 (2)	154 (2)	-	0.07
	0.025	57 (1)	138 (1)	156 (8)	0.09
	0.050	55 (2)	121 (1)	84 (8)	0.12

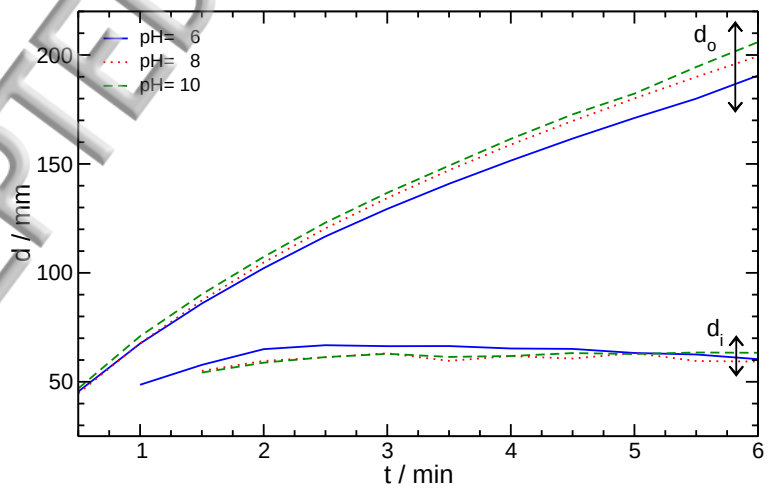

FIG. 4: Time evolution of the precipitate pattern size at selected pH values.

Another possibility to affect fluid motion is changing the convection by altering the density

TABLE III: The influence of flow rate (w) on the characteristics of the precipitate pattern at time t = 4 min, with experimental errors given in brackets. Also listed in the last column is the calculated average height of the underlying gravity current.

w (mL/h)	d_i (mm)	d_o (mm)	N	$\bar{h}$ (mm)
2	22 (1)	68 (1)	68 (8)	0.04
5	31 (1)	92 (1)	84 (8)	0.05
10	43 (2)	118 (1)	92 (8)	0.06
15	51 (1)	128 (1)	120 (8)	0.08
20	57 (1)	138 (2)	120 (4)	0.09
25	63 (1)	152 (2)	128 (16)	0.10
100	88 (2)	175 (1)	136 (12)	0.28

or viscosity difference between the liquids by adding inert materials to the reactant solutions. To increase the density difference between the reactants without significantly modifying solution viscosity, sodium chloride or glycerol is dissolved in the solution with greater density, i.e., in the calcium chloride solution. As a result, the size of the precipitate circles increases, while there is a decline in the number of filaments as the average height of gravity flow decreases from 0.15 mm to 0.10 mm as shown in Table IV. An increase in the density of sodium oxalate solution results in a slightly vertically growing precipitate with greater average height for the gravity current.

When convection is affected by raising both the density and the viscosity of calcium chloride solution with polyvinyl alcohol or polyacrylamide, the viscosity-induced slow down of the gravity current with increasing height dominates the pattern formation as illustrated in Fig. 5. Cellular structures are formed when the dissolved amount of polyacrylamide is increased. First the diameter of the inner circle slightly decreases, then with greater quantity of polyacrylamide added, the growth of the outer circle decelerates, while the radial filaments entirely disappear.

Scanning electron microscopy is used to representatively characterize the microstructure of the solid calcium oxalate particles. The samples are taken from experiments prepared with 0.025 mol/dm^3 sodium oxalate (with pH set to 9) and 4 mol/dm^3 calcium chloride

TABLE IV: The influence of inert material content added to 1 mol/dm^3 calcium chloride solution on the characteristics of the precipitate pattern at time $t = 4$ min, with experimental errors given in brackets. Sodium oxalate concentration is 0.025 mol/dm^3. Also listed in the last column is the calculated average height of the underlying gravity current.

Inert substances		Solution		Pattern			
type	c	ρ (g/cm^3)	η_{rel}	d_i (mm)	d_o (mm)	N	$\bar{h}$ (mm)
reference	–	1.0859	1.27	40.0 (1)	103.0 (1)	-	0.16
NaCl	0.5 mol/dm^3	1.1135	1.36	41.9 (1)	108.0 (1)	30 (1)	0.15
	1 mol/dm^3	1.1214	1.42	42.9 (1)	120.2 (1)	26 (2)	0.12
	2 mol/dm^3	1.1569	1.73	43.7 (1)	133.2 (1)	23 (2)	0.10
glycerol	1 mol/dm^3	1.1063	1.80	43.6 (1)	105.9 (1)	36 (1)	0.15
	2 mol/dm^3	1.1249	2.25	47.0 (1)	112.3 (1)	39 (1)	0.13
PVA	5 g/100 cm^3	1.1177	7.25	50.8 (1)	98.7 (1)	-	0.17
PAA	10 g/100 cm^3	1.1744	4.97	53.6 (1)	97.9 (1)	-	0.18
	20 g/100 cm^3	1.1843	17.84	-	77.5 (1)	-	0.28
	30 g/100 cm^3	1.2176	57.20	-	-	-	-

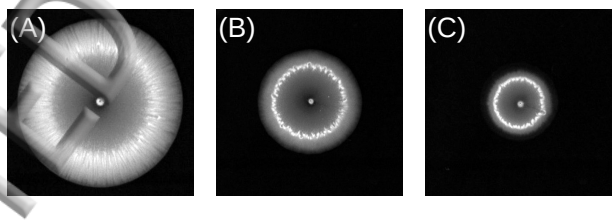

FIG. 5: Precipitate patterns on increasing amount of polyacrylamide (PAA). Chemical composition: $[CaCl_2] = 2$ mol/dm^3, $[Na_2C_2O_4] = 0.025$ mol/dm^3, $\rho_{\mathrm{PAA}} = 10$, 20, and 30 g/100 cm^3 at $t = 4$ min. Field of view: 14 cm $\times$ 14 cm.

solutions at applied flow rate of 20 mL/h. Comparing the flow-driven and the well-stirred reference systems, the first obvious difference is the size of the crystalline particles, as the flow leads to the formation of larger particles. Another distinction is the morphology of the crystalline structures: the reference well-stirred experiments result in rounded and aggregated particles, while samples from the flow-driven patterns contain mostly butterfly or

rose-shaped structures, among other, e.g., octahedron or rectangular crystals. The average size of the rose-shaped are approximately 3 μm, while the butterfly-shaped particles are larger than 5 μm. No spatial variation is found in the structure by scanning various parts of the precipitate pattern, hence uniform distribution of microstructure is associated with the entire the pattern.

To distinguish between the two hydrate forms of calcium oxalate, Raman spectra in the 800–1500 cm^{-1} range are compared.[27] The spectrum of calcium oxalate monohydrate exhibits two peaks at 1463 cm^{-1} and 1490 cm^{-1} belonging to the symmetric C–O bending vibration with the former having greater intensity (see first column of Table V). An additional characteristic peak with smaller intensity is observed at 896 cm^{-1} corresponding to the C–C bending vibration. The spectrum of calcium oxalate dihydrate, however, has only one symmetric C–O bending vibration at 1477 cm^{-1} and the C–C bending vibration is shifted to 911 cm^{-1} as shown in the second column of Table V. The characteristic peaks of the well-stirred reference system (3rd column of Table V) indicate that indeed calcium oxalate monohydrate is produced exclusively in the absence of spatial gradients. In the flow-driven system at high flow rates (100 mL/h) both mono- and dihydrate crystals are identified in the inner circle, while the outer circle richer in precipitates consists mainly of calcium oxalate dihydrate (cf. 4th and 5th columns of Table V). The observed maximum at 1483 cm^{-1} is a result of peak overlapping as the sample contains monohydrate as well.

TABLE V: Reference and experimental Raman band positions calcium oxalate hydrates in decreasing intensity.

reference spectra		experimental results		
calcium oxalate		well stirred	w=100 mL/h	w=100 mL/h
monohydrate (COM)	dihydrate (COD)	system	inner circle	outer circle
1463 cm^{-1}	1477 cm^{-1}	1463 cm^{-1}	1483 cm^{-1}	1483 cm^{-1}
1490 cm^{-1}	911 cm^{-1}	1490 cm^{-1}	1491 cm^{-1}	911 cm^{-1}
896 cm^{-1}		896 cm^{-1}	1461 cm^{-1}	1461 cm^{-1}

The individual crystalline particles are also analyzed by Raman microscopy in samples obtained at moderate flow rate where the mixture of COM and COD can be produced

This manuscript was accepted by J. Chem. Phys. Click here to see the version of record.

simultaneously. Figure 6 confirms the parallel presence of the two hydrate forms. The

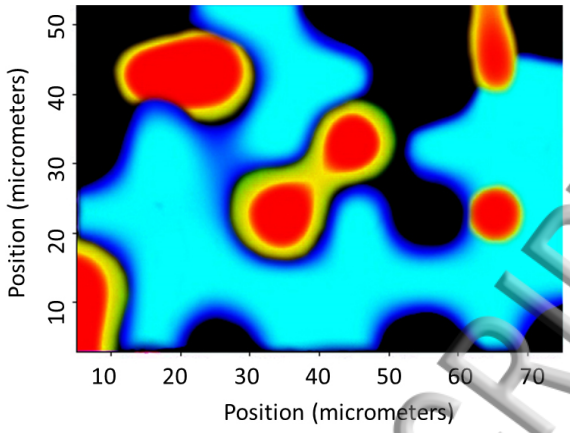

FIG. 6: Spatial distribution map obtained from Raman microscopic measurement of a sample from an experiment with 20 mL/h flow rate. Red regions correspond to COD (intensity at 1477 cm^{-1}) and blue to COM (intensity at 1463 cm^{-1}) in the black background.

Raman spectra of the individual crystalline particles are then used to assign the exact composition. The blue solid curves in Fig. 7 prove that the rectangular crystals are calcium oxalate monohydrate, while the octahedron and the butterfly-shaped particles (red dashed curves) are calcium oxalate dihydrate crystals.

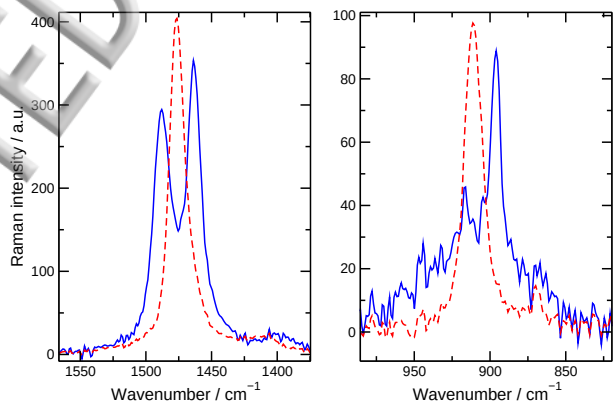

FIG. 7: Raman spectra of the individual particles. The red dashed line corresponds to COD while the blue one to COM.

V. CONCLUSION

We have investigated the precipitate pattern formation in a spatially extended flow-driven system. As calcium chloride solution is pumped into sodium oxalate solution, a thin gravity current spreading on the bottom evolves as a result of the density difference. Effective mixing of the reactants, and hence substantial nucleation, only take place at the leading edge of the current where a large convection roll develops. Even though both nucleation and crystal growth are significantly faster than in the case of copper or cobalt oxalate, the entire precipitate pattern formation is determined by the flow as revealed by the dependence of the descriptors on the characteristics of the gravity current. The unstable stratification of liquid layers behind the tip here also results in the formation of radially expanding filaments, thin regions of downward flow rich in precipitate, although they are not as distinct as in the case of slow precipitate formation of cobalt oxalate. The experiments demonstrate that enhancing the flow by increasing flow rate or the density difference between the reactant solutions, we can control not only the spatial spreading of the precipitate pattern but also the composition of the product. Raman spectroscopic and microscopic measurements completely confirm the presence of the thermodynamically unstable calcium oxalate dihydrate in the experiments with significant gravity current, in sharp contrast to the continuously stirred reference system where only the stable calcium oxalate monohydrate is formed. This flow system therefore can be envisioned as a simple yet efficient method to maintain the concentration gradients in order to keep the system far from equilibrium, which allows the production of a material inaccessible under homogeneous conditions, a thermodynamically unstable crystalline form in this example.

Acknowledgments

This work was financially supported by the European Space Agency (ESTEC 4000102255/11/NL/KML).

[1] J. R. Glauber, *LXXXV. Wie man in diesem Liquore von allen Metallen in wenig Stunden Bume mit Farben soll wachsen machen / How one shall make grow - in this solution, from all metals, in a few hours - trees with color*, Philosophischer Oefen, 186-189 (1661).

[2] R.E. Liesegang, *Ueber einige Eigenschaften von Gallerten*, Naturwissenschaftliche Wochenschrift **30**, 353-363 (1896).

[3] V. Kaminker, J. Maselko, J. Pantaleone, *The dynamics of open precipitation tubes*, J. Chem. Phys. **140**, 244901 (2014).

[4] L.M. Barge, S. S.S. Cardoso, J. H.E. Cartwright et al, *From chemical gardens to chemobrionics*, Chem. Rev. **115**, 8652-8703 (2015).

[5] F. Haudin, J.H.E. Cartwright, F. Brau, A. De Wit, *Spiral precipitation patterns in confined chemical gardens*, Proc. Nat. Acad. Sci. **111**, 17363-17367 (2014).

[6] J. Horváth, I. Szalai, P. De Kepper, *An experimental design method leading to chemical Turing patterns*, Science **324**, 772-775 (2009).

[7] A. Volford, I. Ferenc, M. Ripszám, I. Lagzi, *Pattern formation and self-organization in a simple precipitation system*, Langmuir **23**, 961-964 (2007).

[8] F. Haudin, V. Brasiliense, J.H.E. Cartwright, F. Brau, A. De Wit, *Genericity of confined chemical garden patterns with regard to changes in the reactants*, Phys. Chem. Chem. Phys. **17**, 12804-12811 (2015).

[9] T. Bánsági, V.K. Vanag, I.R. Epstein *Tomography of reaction-diffusion microemulsions reveals three-dimensional Turing patterns*, Science **331**, 1309-1312 (2011).

[10] I. Bena, M. Droz, I. Lagzi, K. Martens, Z. Rácz, A. Volford, *Designed patterns: Flexible control of precipitation through electric currents*, Phys. Rev. Lett. **101**, 075701 (2008).

[11] F. Izsák, I. Lagzi, *A new universal law for the Liesegang pattern formation*, J. Chem. Phys. **122**, 184707 (2005).

[12] R. Makki, X. Ji, H. Mattoussi, O. Steinbock, *Self-Organized Tubular Structures as Platforms for Quantum Dots*, J. Am. Chem. Soc. **136**, 6463-6469 (2014).

[13] R. Makki and O. Steinbock, *Synthesis of Inorganic Tubes under Actively Controlled Growth Velocities and Injection Rates*, J. Phys. Chem. C **115**, 17046-17053 (2011).

[14] I. R. Epstein and J. A. Pojman, *An Introduction to Nonlinear Chemical Dynamics*, Oxford

University Press, Oxford, 1998.

[15] C. Kapral and K. Showalter, *Chemical Patterns and Waves*, Kluwer, Dordrecht, 1995.

[16] S. Thouvenel-Romans, O. Steinbock, *Oscillatory Growth of Silica Tubes in Chemical Gardens*, J. Am. Chem. Soc. **125**, 4338-4341 (2003).

[17] J. Pantaleone, Á. Tóth, D. Horváth, J.R. McMahan, R. Smith, D. Butki, J. Braden, E. Mathews, H. Geri, J. Maselko, *Oscillations of a chemical garden*, Phys. Rev. E **77**, 046207 (2008).

[18] V. Kaminker, J. Maselko, J. Pantaleone, *Chemical precipitation structures formed by drops impacting on a deep pool*, J. Chem. Phys. **137**, 184701 (2012).

[19] Y. Nagatsu, S. Bae, Y. Kato, Y. Tada, *Miscible viscous fingering with a chemical reaction involving precipitation*, Phys. Rev. E **77**, 067302 (2008).

[20] Á. Tóth, D. Horváth, R. Smith, J.R. McMahan, J. Maselko, *Phase diagram of precipitation morphologies in the* Cu^{2+} - PO_4^{3-} *System* J. Phys. Chem. C **111**, 14762-14767 (2007).

[21] L. Rongy, A. DeWit, *Steady Marangoni flow traveling with chemical fronts*, J. Chem. Phys. 124, 164705 (2006).

[22] T. Bansagi, Jr, M.M. Wrobel, S.K. Scott, A.F. Taylor, *Motion and Interaction of Aspirin Crystals at Aqueous-Air Interfaces*, J. Phys. Chem. B **117**, 13572-13577 (2013).

[23] Y-J. Chen, K. Suzuki, K. Yoshikawa, Self-organized target and spiral patterns through the "coffee ring" effect, J. Chem. Phys. **143**, 084702 (2015).

[24] A. Baker, Á. Tóth, D. Horváth, J. Walkush, A. S. Ali, W. Morgan, Á. Kukovecz, J. J. Pantaleone, J. Maselko, *Precipitation pattern formation in the copper(II) oxalate with gravity flow and axial symmetry* J. Phys. Chem. A **113**, 8243-8248 (2009).

[25] E. Tóth-Szeles, G. Schuszter, Á. Tóth, Z. Kónya, D. Horváth, *Flow-driven morphology control in the cobalt-oxalate system*, CrystEngComm, DOI: 10.1039/C5CE02459E (2016).

[26] B. Bohner, G. Schuszter, D. Horváth, Á. Toth, *Morphology control by flow-driven self-organizing precipitation*, Chem. Phys. Lett. **631**, 114 (2015).

[27] B. Bohner, G. Schuszter, O. Berkesi, D. Horváth, Á. Tóth, *Self-organization of calcium oxalate by flow-driven precipitation*, Chem. Commun. **50**, 4289-4291 (2014).

[28] N.Q. Dao, M. Daudon, *Infrared and Raman Spectra of Calculi*, Elsevier, Paris, 1997.

[29] M. Yuzawa, K. Tozuka, A. Tokue, *Effect of citrate and pyrophosphate on the stability of calcium oxalate dihydrate* Urol. Res. **26**, 83-88 (1998).

[30] L. Lepage, R. Tawashi, *Growth and Characterization of Calcium Oxalate Dihydrate Crystals (Weddellite)* J. Pharm. Sci. **71**, 1059-1062 (1982).

[31] F. Grases, A. Millan, A. Conte, *Production of calcium oxalate monohydrate, dihydrate, or trihydrate* Urol. Res. **18**, 17-20 (1990).

[32] S. Kotrlỳ, L. Šůcha, *Handbook of chemical equilibria in analytical chemistry*, Ellis Horwood Limited, 1985.

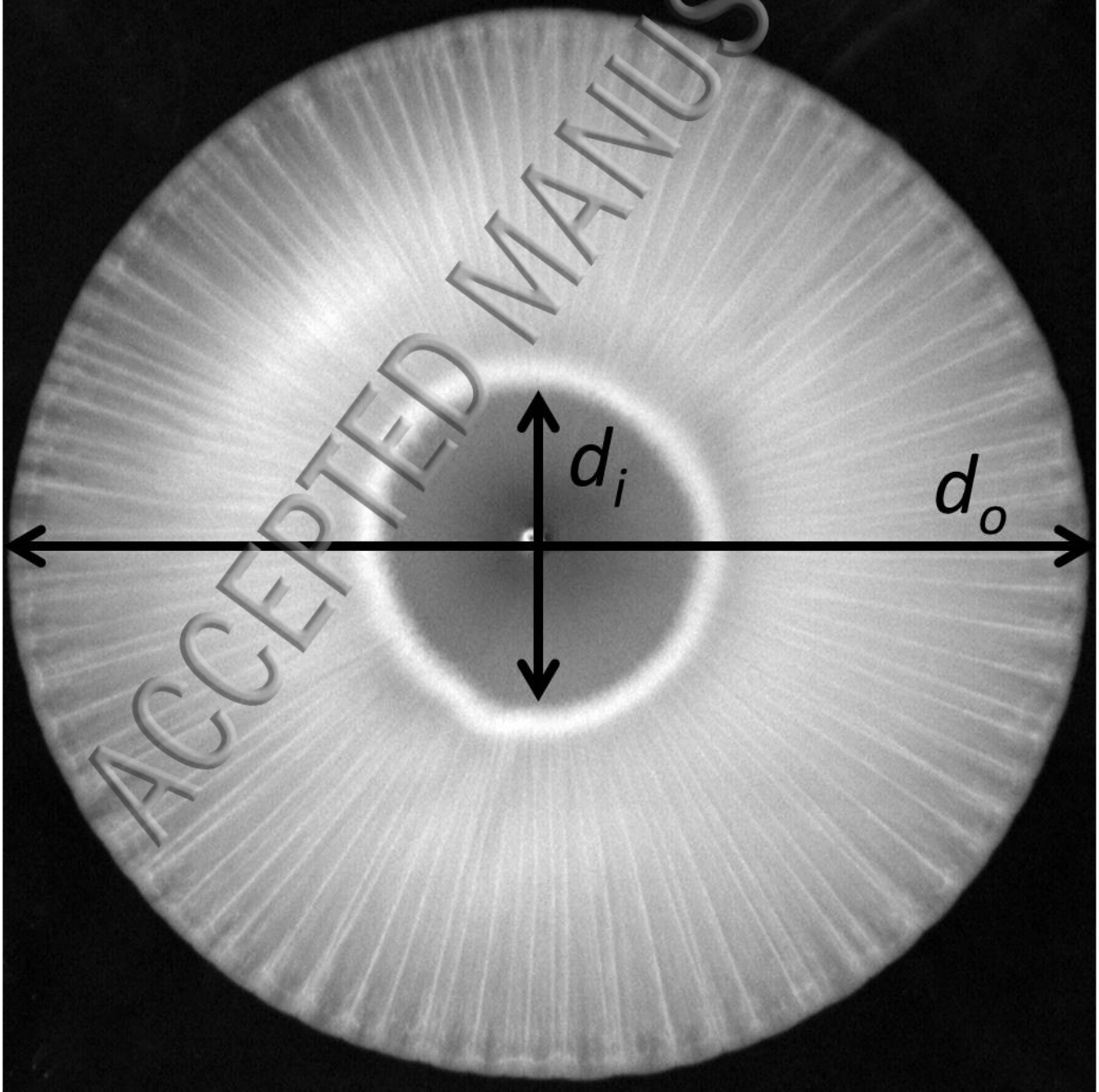

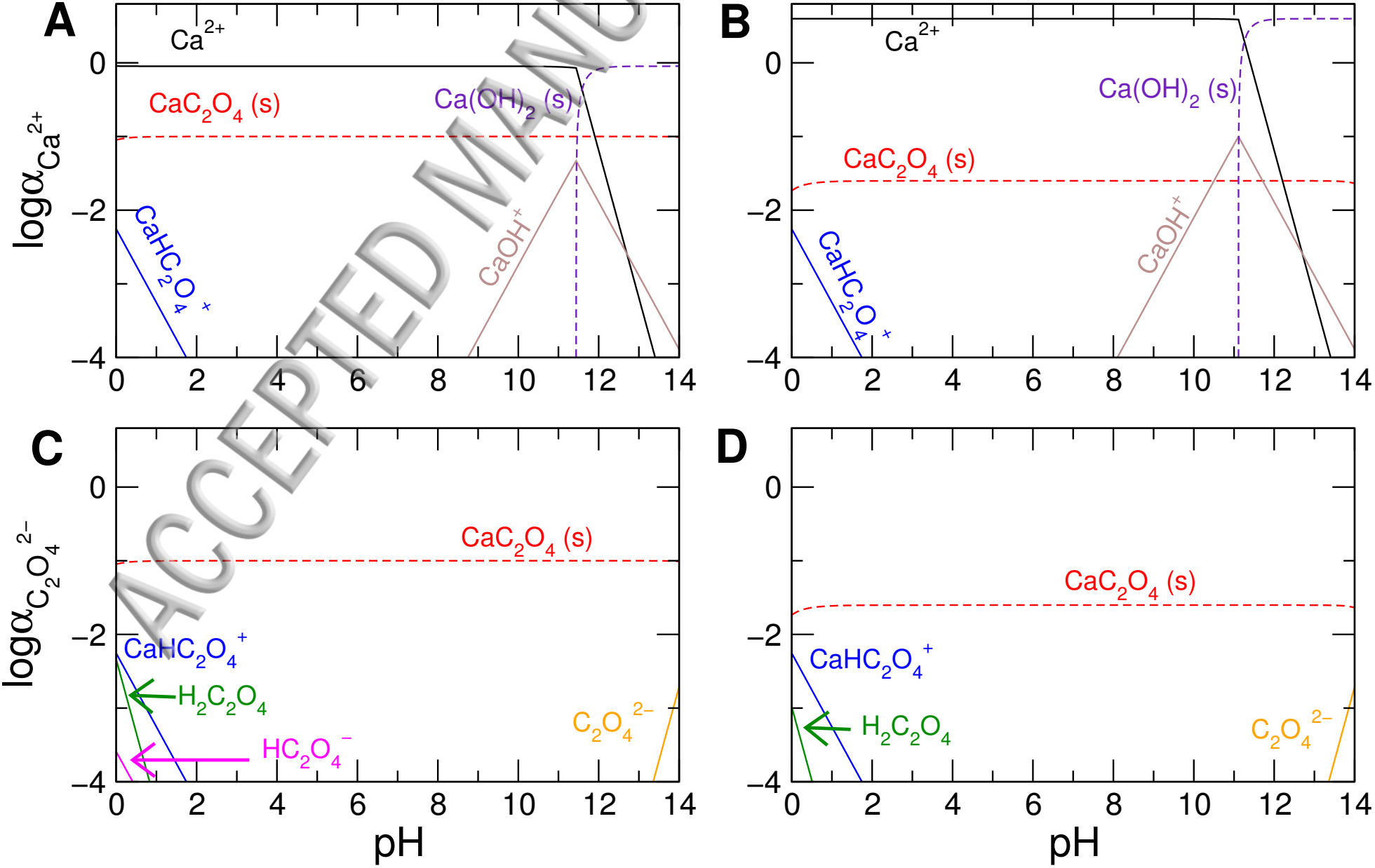

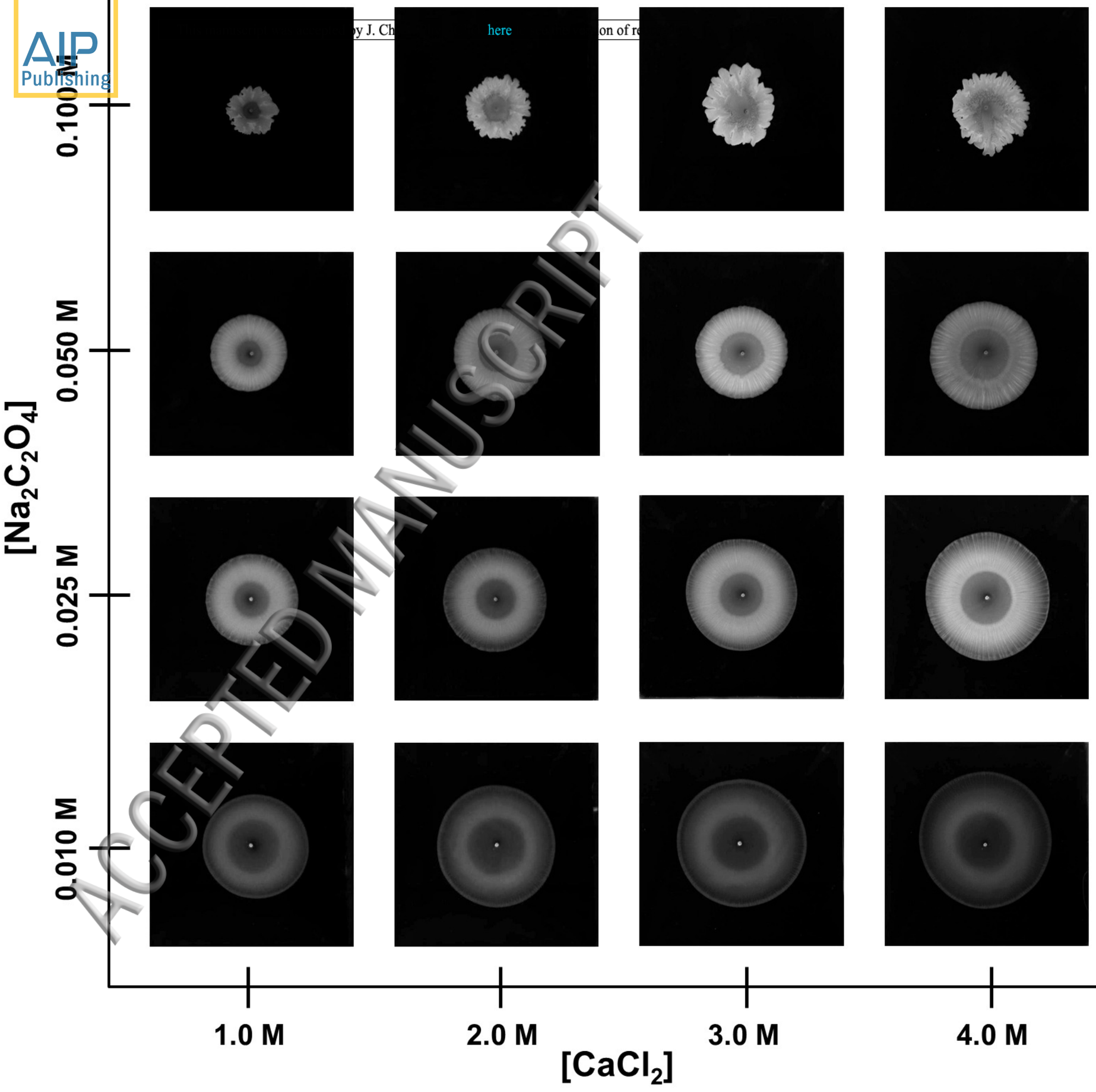

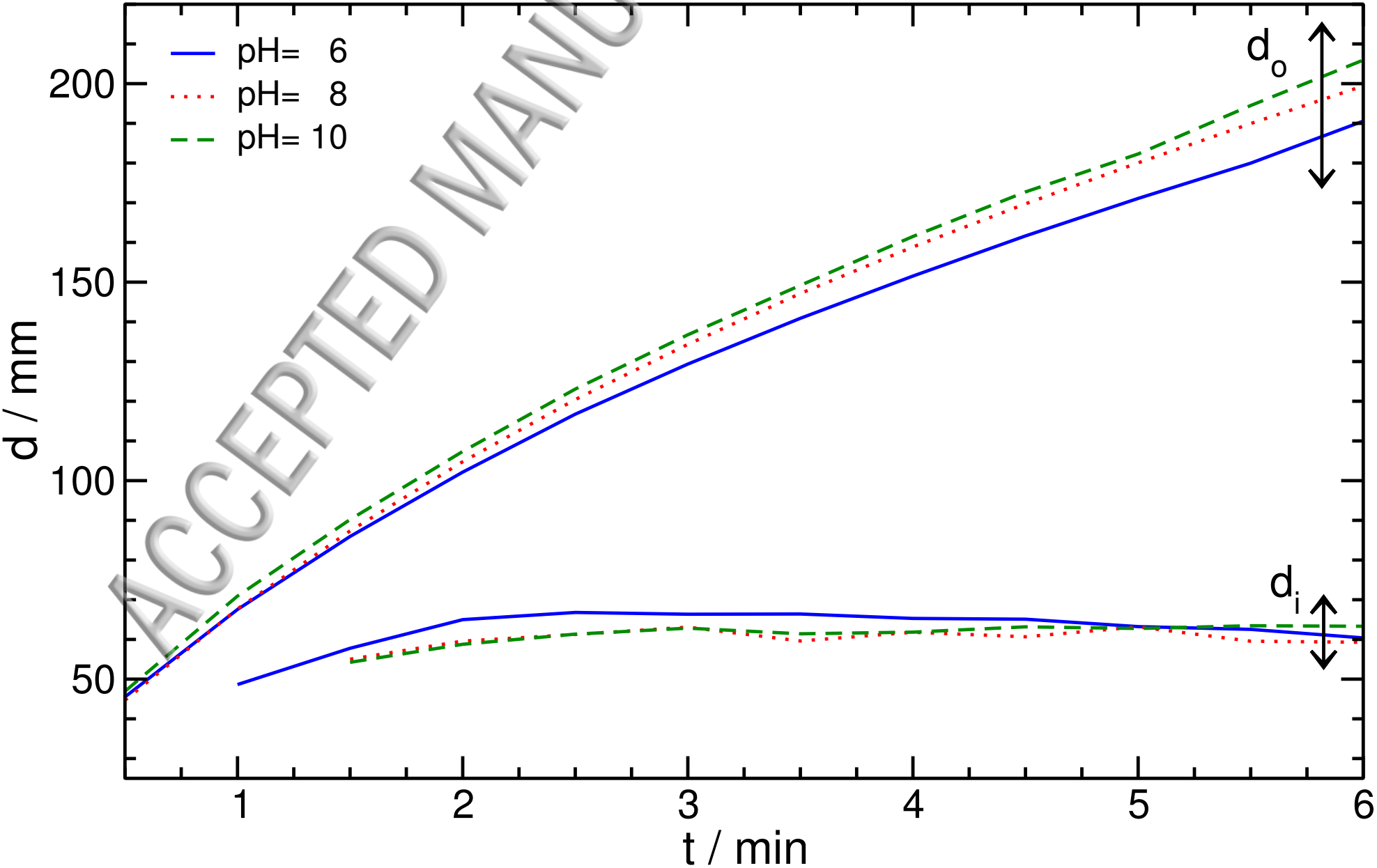

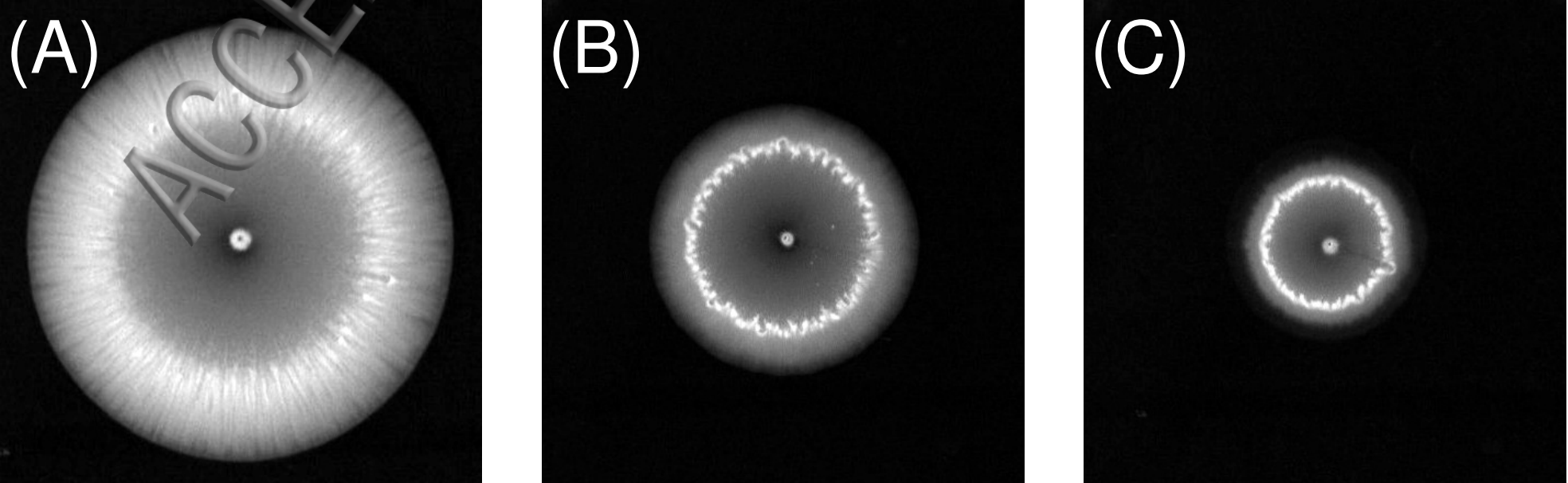
(A)
(B)
(C)

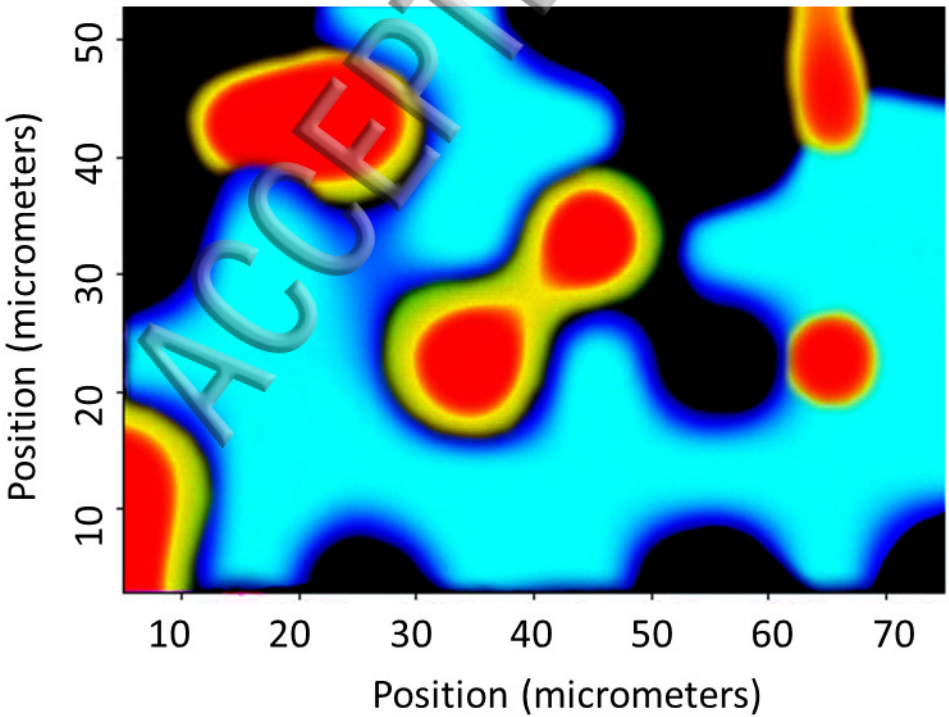
Position (micrometers)
10
20
30
40
50
Position (micrometers)
10
20
30
40
50
60
70